Cockroaches traverse crevices, crawl rapidly in confined spaces, and inspire a soft, legged robot

Kaushik Jayaram[a] and Robert J. Full[a,1]

[a]Department of Integrative Biology, University of California, Berkeley, CA 94720

Jointed exoskeletons permit rapid appendage-driven locomotion but retain the soft-bodied, shape-changing ability to explore confined environments. We challenged cockroaches with horizontal crevices smaller than a quarter of their standing body height. Cockroaches rapidly traversed crevices in 300–800 ms by compressing their body 40–60%. High-speed videography revealed crevice negotiation to be a complex, discontinuous maneuver. After traversing horizontal crevices to enter a vertically confined space, cockroaches crawled at velocities approaching 60 cm·s^{-1}, despite body compression and postural changes. Running velocity, stride length, and stride period only decreased at the smallest crevice height (4 mm), whereas slipping and the probability of zigzag paths increased. To explain confined-space running performance limits, we altered ceiling and ground friction. Increased ceiling friction decreased velocity by decreasing stride length and increasing slipping. Increased ground friction resulted in velocity and stride length attaining a maximum at intermediate friction levels. These data support a model of an unexplored mode of locomotion—"body-friction legged crawling" with body drag, friction-dominated leg thrust, but no media flow as in air, water, or sand. To define the limits of body compression in confined spaces, we conducted dynamic compressive cycle tests on living animals. Exoskeletal strength allowed cockroaches to withstand forces 300 times body weight when traversing the smallest crevices and up to nearly 900 times body weight without injury. Cockroach exoskeletons provided biological inspiration for the manufacture of an origami-style, soft, legged robot that can locomote rapidly in both open and confined spaces.

locomotion | exoskeleton | crawling | confined | soft robotics

The emergence of terradynamics (1) has advanced the study of terrestrial locomotion by further focusing attention on the quantification of complex and diverse animal–environment interactions (2). Studies of locomotion over rough terrain (3), compliant surfaces (4), mesh-like networks (5), and sand (6–8), and through cluttered, 3D terrain (9) have resulted in the discovery of new behaviors and novel theory characterizing environments (10). The study of climbing has led to undiscovered templates (11) that define physical interactions through frictional van der Waals adhesion (12, 13) and interlocking with claws (14) and spines (5). Burrowing (15, 16), sand swimming (17), and locomotion in tunnels (18) have yielded new findings determining the interaction of bodies, appendages, and substrata.

Locomotion in confined environments offers several challenges for animals (18) that include limitations due to body shape changes (19, 20), restricted limb mobility (21), increased body drag, and reduced thrust development (22). Examining the motion repertoire of soft-bodied animals (23), such as annelids (19), insect larvae (24), and molluscs (25), has offered insight into a range of strategies used to move in confined spaces. Inspiration from soft-bodied animals has fueled the explosive growth in soft robotics (26–30), which is not only creating new perspectives in robot design and control, but also more sharply defining the advantages and disadvantages of soft systems capable of maneuvering in constrained environments. As pointed out by Kim et al. (26), "soft materials also lend themselves to highly flexible and deformable structures, providing additional functional advantages to animals,

such as enabling entrance into small apertures for shelter or hunting." However, disadvantages include weight support against gravity, body/appendage control, and "high deformability and energy-absorbing properties of soft tissues prevent[ing] them from exerting large inertial forces and limit[ing] how fast soft animals can move from place to place" (26).

We explored the capability of cockroaches to not only exploit the advantages of appendages with structures that allow effective interaction with diverse terradynamic surfaces, but that also permit them to function as exceptional soft-bodied locomotors in confined spaces. Cockroaches use rigid, jointed exoskeletons to run rapidly at speeds approaching 1.5 m·s^{-1} (31), climb up walls (11, 32), race along ceilings (33), and swing stealthily under ledges out of sight (34). However, materials science has revealed that the stiffness of exoskeletal tissue can differ by eight orders of magnitude (35–38), permitting the possibility that cockroaches with powerful propulsive appendages might also retain the advantages of soft-bodied animals capable of conforming to their environment (39). As yet, no study has quantified cockroaches' capacity to traverse crevices and crawl in confined spaces.

We selected the American cockroach, *Periplaneta americana*, because of its high speed (31), maneuverability (34, 40), robustness (41), and tenacity to enter and leave spaces. To determine the smallest horizontal crevice that a cockroach could traverse, we challenged animals with a series of decreasing crevice heights. We hypothesized a minimum height based on compression tests of body segments.

Once cockroaches entered the confined space and became more sprawled, we hypothesized that running velocity, stride length, and

---

Significance

Cockroaches intrude everywhere by exploiting their soft-bodied, shape-changing ability. We discovered that cockroaches traversed horizontal crevices smaller than a quarter of their height in less than a second by compressing their bodies' compliant exoskeletons in half. Once inside vertically confined spaces, cockroaches still locomoted rapidly at 20 body lengths per second using an unexplored mode of locomotion—body-friction legged crawling. Using materials tests, we found that the compressive forces cockroaches experience when traversing the smallest crevices were 300 times body weight. Cockroaches withstood forces nearly 900 times body weight without injury, explaining their robustness to compression. Cockroach exoskeletons provided inspiration for a soft, legged search-and-rescue robot that may penetrate rubble generated by tornados, earthquakes, or explosions.

stride period would decrease with crevice height, whereas slipping and the probability of a zigzag path would increase. We used high-speed movie to quantify the kinematics of crawling, postural changes

of sprawl angle, and foot or tarsal position relative to free running (31, 42). Motivated by studies of the role of body friction during undulatory swimming in frictional fluids by sandfish lizards (17,
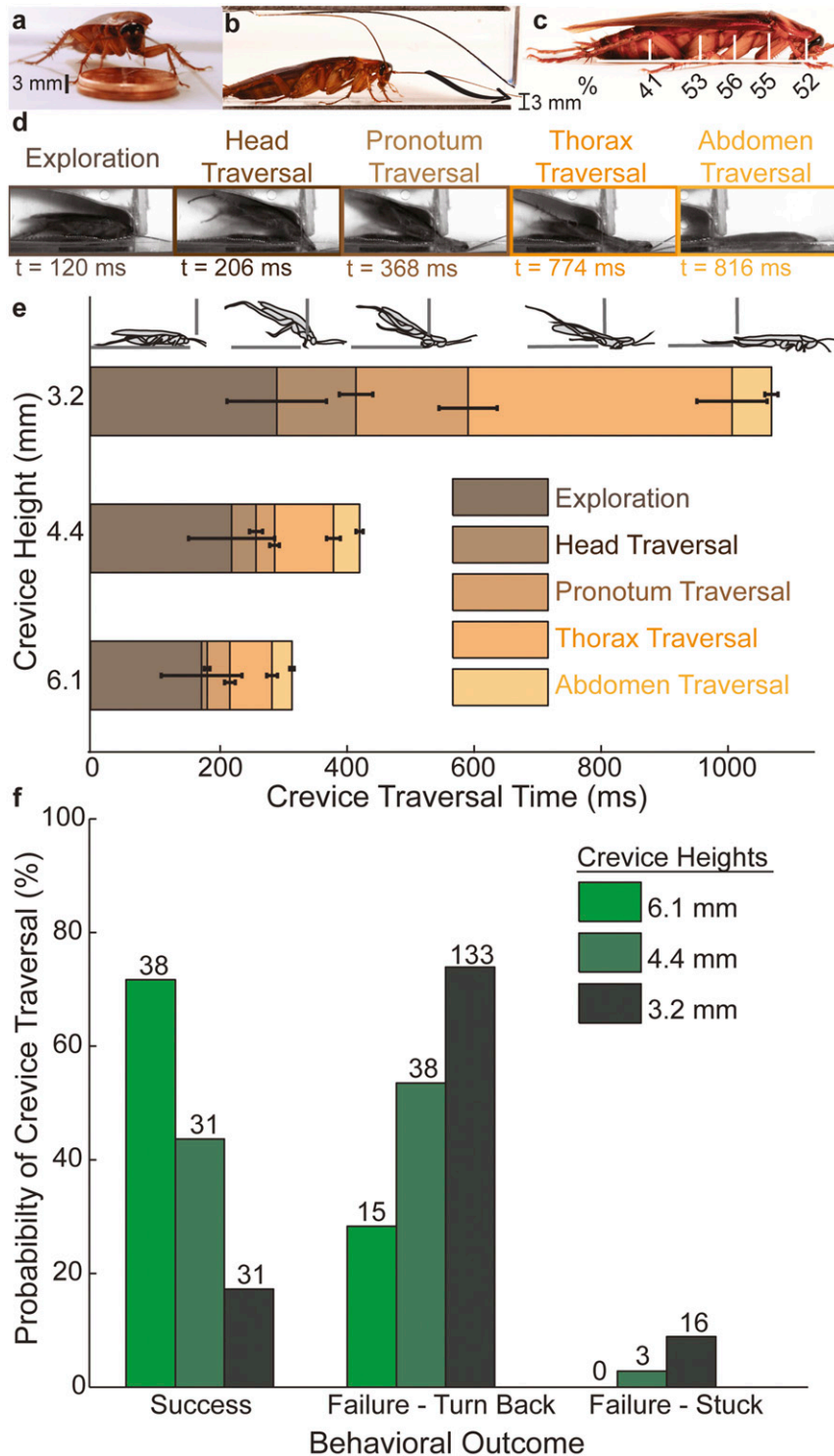

Fig. 1. Performance of cockroaches traversing horizontal crevices. (*A*) Comparison of freestanding height of American cockroach, *Periplaneta americana*, relative to the near-minimum crevice height traversed equal to 3 mm, two stacked pennies. (*B*) Crevice traversal apparatus with cockroach about to enter (Fig. S1A). (*C*) Body compression (white vertical bars) resulting from a 100-g load across segment. Percent body compression shown below segment (Fig. S1C and Table S1). (*D*) Crevice traversal stages extracted from high-speed movie frames with corresponding time stamp for 3-mm height (Movie S1). (*E*) Crevice traversal time at three crevice heights. Each behavioral stage duration is stacked onto the next from left to right to also show total time. Points and error bars represent mean ± 1 SD. (*F*) Probability of crevice traversal for three crevice heights (represented by three colors). Cockroaches successfully traversed the greatest heights more frequently and failed to traverse the lowest crevice heights by turning back or getting stuck within the crevice. Number of trials is shown above bar.

43) and the thrust produced by flipper-driven surface locomotion by sea turtle hatchlings (8), we varied ceiling and ground friction to determine their effect on confined-space crawling performance. Given these results, we created a model of this unexplored mode of locomotion in which drag acts on an animal's dorsal and ventral surface, but the media does not flow around the animal.

Finally, we hypothesized that compression of the body and legs would demonstrate nonlinear, viscoelastic behavior (41), suggesting crevice crossing might be affected by rate and that the magnitude of peak compression forces would reveal the extent of exoskeletal robustness. As a first step toward quantifying the exoskeletal material properties (41) and shape changes that enable cockroaches to traverse crevices and crawl in confined spaces, we measured the compression of selected head and body segments by adding loads to anesthetized animals and performed a series of dynamic compressive cycle tests on living animals.

Inspired by the data on cockroach segment and body compression, postural change, and kinematics, we designed a legged robot using the smart composite microstructure (SCM) manufacturing (44–46) approach involving laser-cutting, laminating, and the folding of exoskeleton-like plates. We see this robot useful both as a physical model to test future hypotheses of the mechanisms permitting confined-space locomotion, as well as a first step toward the development of a soft search-and-rescue robot that can penetrate the rubble left by tornados, earthquakes, or explosions.

Results and Discussion

Crevice Traversal. The American cockroach (0.76 ± 0.16 g; 31.10 ± 2.16-mm length; 12.52 ± 1.48-mm height), *Periplaneta americana*, traversed horizontal crevices as small as 3 mm, the height of two stacked US pennies (Fig. 1 *A* and *B*). A vertically adjustable acrylic gate mounted on a precision linear stage permitted control of crevice height (± 0.05 mm; Fig. 1*B*, *SI Methods*, and Fig. S1*A*). To set experimental crevice height, we directly measured body compression of freshly anesthetized animals from their abdomen to head while positioned on a flat surface by suspending a load greater than 100 times body weight across each section (Fig. 1*C*, Fig. S1*C*, and Table S1). Exoskeletal sections were all highly compressible, ranging from 41% to 57% of normal with the load resulting in no injury.

Crevice traversal was rapid (288- to 821-ms interquartile range) and, to the naked eye, appeared continuous. High-speed videography revealed crevice traversal to be a complex behavior involving several stages (Fig. 1*D* and Movie S1). We defined these stages to enable measurement of the time taken to progress through each stage at the three crevice heights. (*i*) Exploration and crevice detection: Once placed within the apparatus (Fig. 1 *B* and *D*), the animals used their antennae to explore their surroundings and searched for escape openings. If one or both antennae passed through the crevice, the animal reoriented itself to ensure both antennae were extending out of the crevice and continued tactile exploration. We suspect this searching behavior enabled the cockroaches to estimate the size of the crevice and to determine whether the other side was safe for escape. (*ii*) Head traversal with entry and body orientation: On completion of crevice detection, the cockroach typically paused briefly and rammed into the crevice head-first multiple times, often hitting the gate, before pitching downward to the enter the crevice. For larger crevice sizes (6 mm and above), this would be immediately followed by abdominal traversal with little body compression. During this phase, the legs rapidly cycled attempting to grip surfaces and generate sufficient friction. In concert with head entry, the front legs stretched outside the crevice attempting to pull the body through. At the same time, the remainder of body pitched upward, allowing the middle and hind legs to push off the side/top walls of the chamber. (*iii*) Pronotum traversal: As the leg movements began getting restricted (especially the front legs), the body rapidly rolled from side to side accompanied by leg pushing. The rapid body rotations possibly

helped to reorient the middle and hind legs for maximizing thrust production (47) and to potentially passively align the body with respect to the crevice opening. (*iv*) Thorax traversal: We hypothesized this to be one of most challenging stages with the highest chance of failure by getting stuck due to the body morphology (Table S1). The movement of the legs was severely restricted, and the animal was likely experiencing large normal forces. Animals made forward progress primarily by thrusting their hind legs. (*v*) Abdomen traversal: After thorax traversal, the body was again reoriented into a "flat" position (body pitch of 0°). The front legs and middle legs were free to operate, whereas hind-leg movement was restricted, making progression difficult. The compressibility of the abdomen appeared to reduce the normal load on the body, enabling the animal to generate thrust sufficient to successfully negotiate the crevice.

The time taken from head entry until abdomen tip exit increased with a decrease in crevice height from 6.1 to 3.2 mm [ANOVA, $P < 0.001$, $F_{(2,94)} = 88.9$; Fig. 1*E*]. Traversal time was similar for 6.1- and 4.4-mm crevices (0% and $27 \pm 3\%$ abdomen compression, respectively; post hoc analysis, Tukey's honest significant difference), but significantly longer at 3.2 mm ($47 \pm 3\%$ abdomen compression), approaching the limit of performance. Consistent with this conclusion, the probability of successful crevice traversal decreased significantly with a decrease in crevice height from $72 \pm 5\%$ at 6.1 mm to just $17 \pm 3\%$ at 3.2 mm [Cochran–Mantel–Haenszel, $P < 0.001$, $\chi^2_{(2)} = 44.8$; Fig. 1*F*]. Turning back during a trial was the dominant failure mode, suggesting that animals seek alternate routes if crevices are too small, presumably using sensory feedback (48). Animals were never trapped in the largest crevices, but occasionally became stuck at the smallest crevice heights ($9 \pm 2\%$) during thorax traversal, a potentially fatal event in nature if exposed to predators.

Confined-Space Crawling. After traversing narrow crevices, cockroaches crawled rapidly in spaces confined vertically by two stacked horizontal plates (*SI Methods* and Fig. S1*B*) at velocities approaching 60 cm·s⁻¹, despite body compression and large postural changes such as sprawl angle (Movie S2). High-speed kinematic analysis of marked animals at four ceiling heights (Fig. 2 *A* and *B*) revealed that velocity [58.05 ± 2.33 cm·s⁻¹, ANOVA, $P = 0.56$, $F_{(2,72)} = 4.72$] did not vary significantly across the three greatest ceiling heights, and only decreased at the smallest height where animals experienced the greatest body compression and friction [4 mm; 14.52 ± 0.98 cm·s⁻¹; ANOVA, $P < 0.001$, $F_{(3,96)} = 14.72$; Fig. 2*C*]. Effective stride length explained the changes in velocity, whereas stride period remained constant across all crevice sizes [61.05 ± 6.06 ms, $P = 0.34$, $F_{(3,96)} = 1.28$]. Ceiling height constrained posture by increasing sprawl angle proportionally [$P < 0.001$, $F_{(3,96)} = 24.12$; Fig. 2*B*]. Surprisingly, the distance from the foot to the body midline, as viewed from the top (tarsus midline distance), did not change significantly across ceiling heights [11.89 ± 0.96 mm; $P = 0.64$, $F_{(3,96)} = 3.61$; Fig. 2*C*]. This foot placement is similar to that most effective for maximizing ground thrust as predicted from cockroach musculoskeletal models (49). Cockroaches used an alternating tripod gait at all ceiling heights except the smallest where the gait became irregular with the middle legs often applying force in synchrony to thrust the body forward. Consequently, at the smallest ceiling height, animals were unable to follow straight-lined paths [decreased tortuosity index; $P = 0.002$, $F_{(3,96)} = 5.49$; Fig. 2*C*]. Foot slippage also increased at the smallest ceiling height [decreased stride success ratio; $P = 0.005$, $F_{(3,96)} = 3.31$; Fig. 2*C*]. The ability of cockroaches to maintain performance with minimal changes in kinematic parameters at the three greatest ceiling heights is similar to outcomes in experiments with ferrets running in tunnels with back height reduced by 40% and hip height by 25% (50). However, at the smallest ceiling heights, results for confined-space crawling suggest that cockroaches were attempting to generate sufficient thrust through ground engagement, but because of
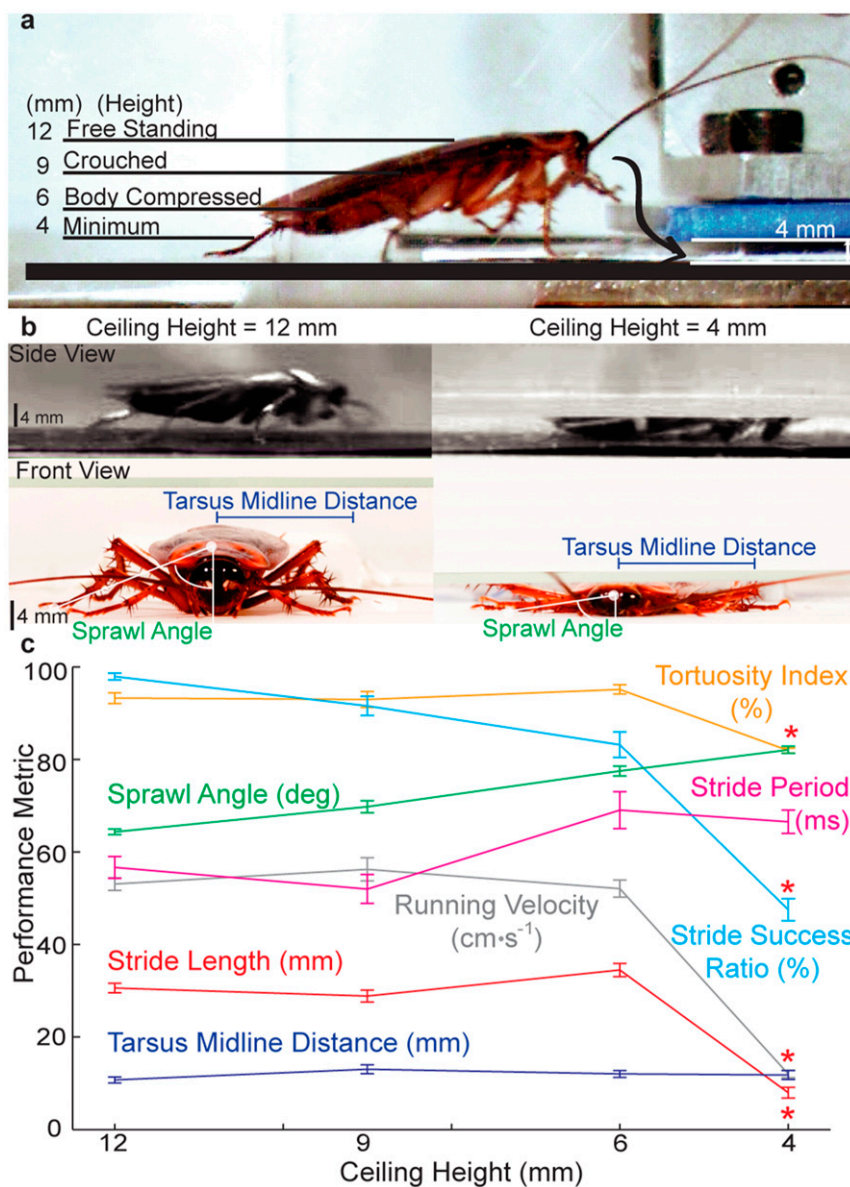
Fig. 2. Confined-space crawling performance of cockroaches. (*A*) Crevice crawling apparatus with cockroach about to enter (Fig. S1). Ceiling heights used represent freestanding (12 mm), crouched (9 mm), just beginning to compress body (6 mm), and minimum ceiling height within which animals crawled (4 mm). (*B*) Side (from movie) and front view of cockroach crawling within chamber at two ceiling heights. Front view shows the increase in sprawl angle, but not foot-to-body midline distance (tarsus midline distance) as ceiling height was reduced. (*C*) Performance metrics, velocity (gray), stride length (red), stride period (magenta), sprawl angle (green), tarsus midline distance (dark blue), stride success ratio (ratio of successful strides with no foot slipping relative to the total number of strides; light blue), and tortuosity index (forward displacement of cockroach relative to the length of the actual path taken; orange) as a function of ceiling height with their respective units are indicated in parentheses after label. Points and error bars show mean ± 1 SD. Red stars represent a significant difference at 4 mm relative to larger ceiling heights.

body contact with the ground and ceiling were operating in a "friction-limited" environment. Under these conditions, thrust on the body is expected to equal the maximum friction force offered by the surface because of foot slippage.

Body-friction legged crawling operates in a unique regime where drag is exerted on the body, friction dominates thrust, but the media does not flow. To determine whether cockroaches undergo confined-space, body-friction legged crawling, we varied the ground and ceiling friction of the apparatus (Fig. 3). We directly measured the coefficients of friction using anesthetized animals interacting with different surfaces to produce three levels of friction for both the ceiling (fivefold change) and ground (twofold change; *SI Methods* and Table S2). We hypothesized that increased ceiling friction and dorsal drag would decrease velocity by

decreasing stride length and increasing slipping (reduce stride success ratio). At the smallest crevice height (4 mm), an increase in ceiling friction significantly decreased mean velocity [$P < 0.001$, $F_{(2,72)} = 37.87$; Fig. 3*B*]. The decrease in velocity can be explained by a decrease in stride length [$P < 0.001$, $F_{(2,72)} = 122.58$] and an increase in foot slippage [decrease in stride success ratio; $P < 0.001$, $F_{(2,72)} = 48.16$]. Stride period remained unaffected by ceiling friction [$P = 0.1$, $F_{(2,72)} = 7.27$]. For an increase in ground friction, we hypothesized that the trend in these locomotor variables would depend on the differential effect of ventral body drag versus an increased thrust from greater leg purchase. At the smallest crevice height (4 mm), an increase in ground friction significantly increased mean velocity at medium friction levels [$P < 0.001$, $F_{(2,69)} = 73.4$] compared with both the low and high
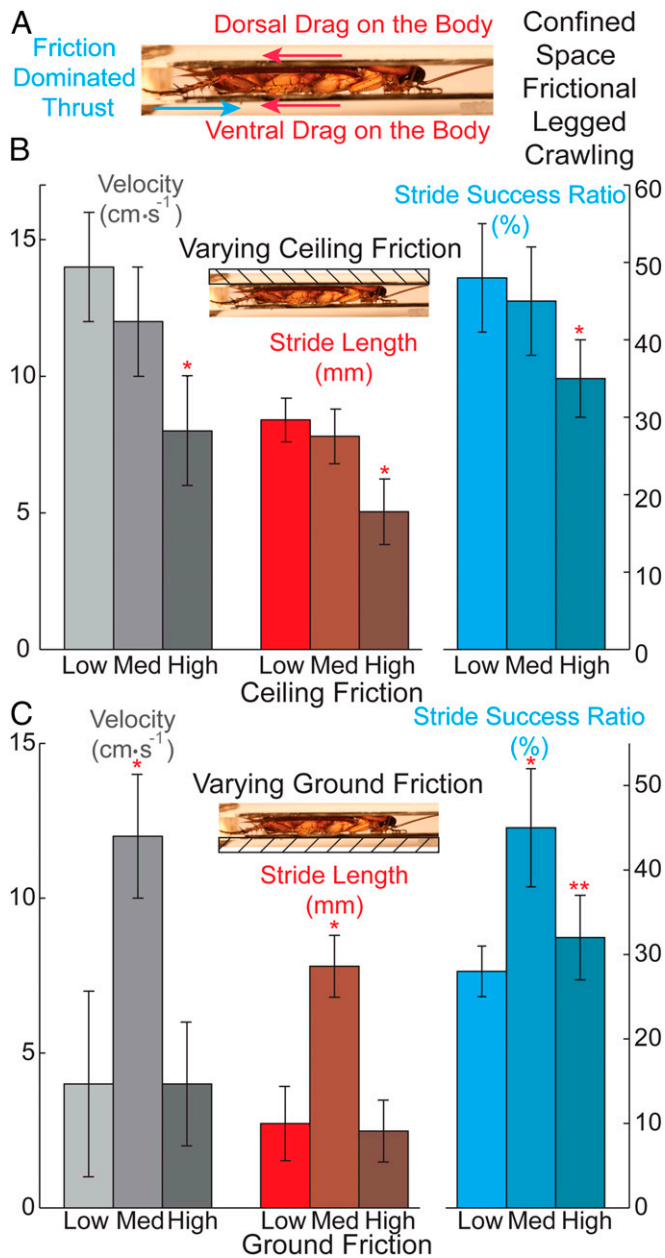
Fig. 3. Effects of varying ground and ceiling friction for confined-space crawling performance. (A) Confined-space body-friction legged crawling characterized by drag on the dorsal and ventral surface of the body and friction-dominated thrust by legs in a nonflowing medium. (B) Performance metrics, velocity (grays), stride length (red-brown), and stride success ratio (blues) at 4-mm ceiling height (respective units indicated in parentheses below label) as a function of ceiling kinetic friction varied at three levels (low, medium, and high) with ground kinetic friction constant. (C) Performance metrics, velocity (grays), stride length (red-brown), and stride success ratio (blues) at 4-mm ceiling height (respective units indicated in parentheses below label) as a function of ground kinetic friction varied at three levels (low, medium, and high) with ceiling kinetic friction constant. Bars show mean ± 1 SD. Red stars represent a significant difference from other kinetic friction levels.

conditions (Fig. 3C). Stride length [$P < 0.001$, $F_{(2,69)} = 246.7$] and stride success ratio [foot slippage; $P < 0.001$, $F_{(2,69)} = 89.10$] showed a similarly significant trend with a performance peak at the medium friction condition. Stride period remained unaffected by changes in ground friction [$P = 0.07$, $F_{(2,69)} = 12.36$]. Results from an increase in ground friction imply a trade-off between

increasing leg thrust and increasing body drag. Therefore, confined-space crawling in cockroaches appears to have features of both the body friction of undulatory swimming in frictional fluids as seen in sand-swimming lizards (17, 43) and the thrust produced by flipper-driven surface locomotion produced by sea turtle hatchlings (8) except that in crevices the surrounding media do not flow (Fig. 3A). Body-friction legged crawling deserves further attention.

Model of Body-Friction Legged Crawling. To begin to explain our experimental results and to generate further hypotheses concerning the effect of friction on confined-space crawling, we made a model with few fitting parameters (Fig. 4A; see *Supporting Information* for detailed description). The model consists of a compliant body confined between two parallel plates and actuated by a single leg. All animal–environment interactions are characterized by normal and tangential forces governed by Amonton's and Coulomb's laws of dry friction (51). Due to the lack of direct leg force measurements during confined crawling, we chose to model the cockroach leg as a linear force–velocity actuator (ref. 52, equation 1; *Supporting Information*, Eq. S13) motivated by studies of leg press tasks in humans (52), where the leg force and velocity can be
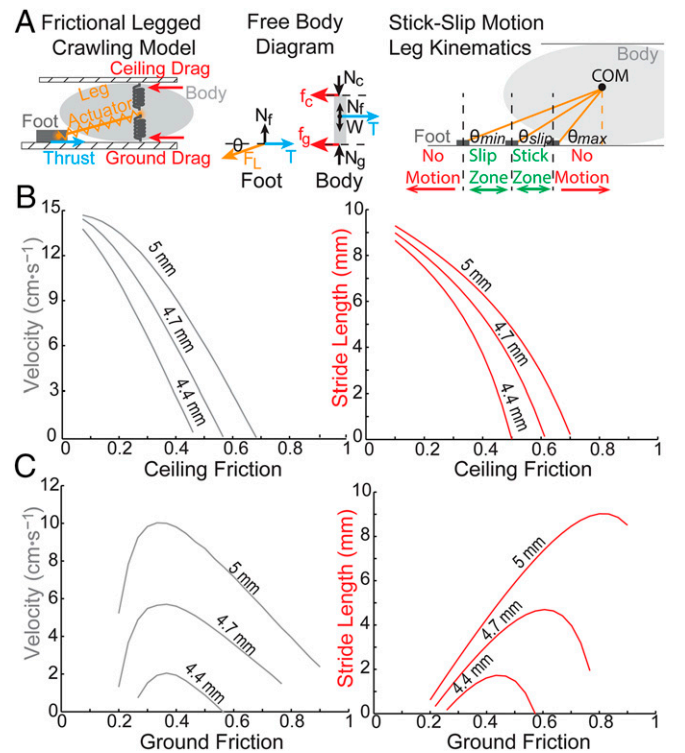

Fig. 4. Model of body-friction legged crawling. (A, Left) Model simplified representation of a cockroach in a confined space depicted as a compressible body (light gray solid oval) with a single leg (wavy tan line) ending in a foot (dark gray box) confined within two parallel plates (hashed boxes). (Center) Free body diagram of foot and body. Leg force (F_L) is indicated in tan, thrust (T) in blue, drag—ceiling (f_c) and ground (f_g)—in red, body weight (W), and all normal forces—ceiling–body (N_c), ground–body (N_g), and ground–foot (N_f)—in black. (Right) Foot positions, where forward body displacement occurs with (slip zone) and without (stick zone) foot slippage, are marked in green, whereas positions where no body motion is possible are indicated in red. Leg orientations at the above-foot positions—slip angle (transition from stick to slip, θ_{slip}) and the maximum (θ_{max}) and minimum (θ_{min}) angle to overcome body drag are indicated. (B) Performance metrics, velocity (gray) and stride length (red) at three ceiling heights (4.4, 4.7, and 5 mm) as a function of ceiling kinetic friction with ground kinetic friction constant. (C) Performance metrics, velocity (gray), and stride length (red) at three ceiling heights (4.4, 4.7, and 5 mm) as a function of ground kinetic friction with ceiling kinetic friction constant.

approximated to vary linearly. The motion of the body is separated into two distinct phases—"stick" and "slip." During stick phase (*Supporting Information*, Eqs. S8 and S9), maximum foot–ground friction is greater than the magnitude of the horizontal component of leg force, so the foot holds in place. As a result, the leg actuator displacement directly yields body displacement (*Supporting Information*, Eq. S10) and velocity (*Supporting Information*, Eq. S17). However, during slip phase, foot–ground friction is insufficient to prevent the foot from slipping backward relative to the body (*Supporting Information*, Eqs. S11 and S12). Body displacement and velocities are therefore computed by integrating net force (difference between thrust and drag) over the slip duration. The extent of leg excursions in stick and slip mode detailed in *Supporting Information* are illustrated in Fig. 4A. We used our measurements of friction coefficients (Table S2), normal (compressive) forces (Fig. 5B), maximum leg length (30 mm), and velocity (0.5 m·s⁻¹), to predict stride length and mean body velocity for comparison with our experimental results (Figs. 3 B and C, and 4 B and C). We estimated maximum leg force from data on a related cockroach species (53). Computed body displacements during the stick phase were significantly longer than the slip phase at small crevice heights or high friction conditions, matching our experimental observations.

In accordance with our experimental data (Fig. 3B), the model indicates that increasing ceiling friction monotonically increases the overall resistance due to friction-based drag and, therefore, reduces forward velocity by decreasing stride length (Fig. 4B).

The model suggests that smaller crevice heights are likely to decrease performance at a given ceiling friction. Furthermore, the model indicates that maximal forward velocity and stride length occur at intermediate ground friction conditions, because the magnitude of thrust depends on the differential friction between the foot and body (Fig. 4C). As in ceiling friction results, the model suggests that smaller crevice heights are likely to decrease performance at a given value of ground friction.

Although results from our initial model follow trends observed in experimental measurements, the model reveals at least three areas of future study for body-friction legged crawling. First, an improved understanding of foot contact mechanics is needed to provide insight into the complexities of thrust generation beyond simple coulomb friction-type attachments that include interlocking (14, 54, 55), adhesion (56–58), and resistive forces in granular media (7, 59). Second, a leg actuation model that more effectively captures dependence of force production on such factors such as leg morphology, lever and transmission systems, and muscle mechanics (21). Finally, a more developed quantification of body and leg kinetic friction as they relate to contact geometry and exoskeletal material properties could improve estimates and reveal principles underlying the interesting complexity of the stick–slip interactions as a novel locomotor challenge for both animals (and robots). Incorporating these biologically relevant measurements into our initial model will move us closer to generating predictions concerning the habitats and environments animals might exploit using body-friction legged crawling.
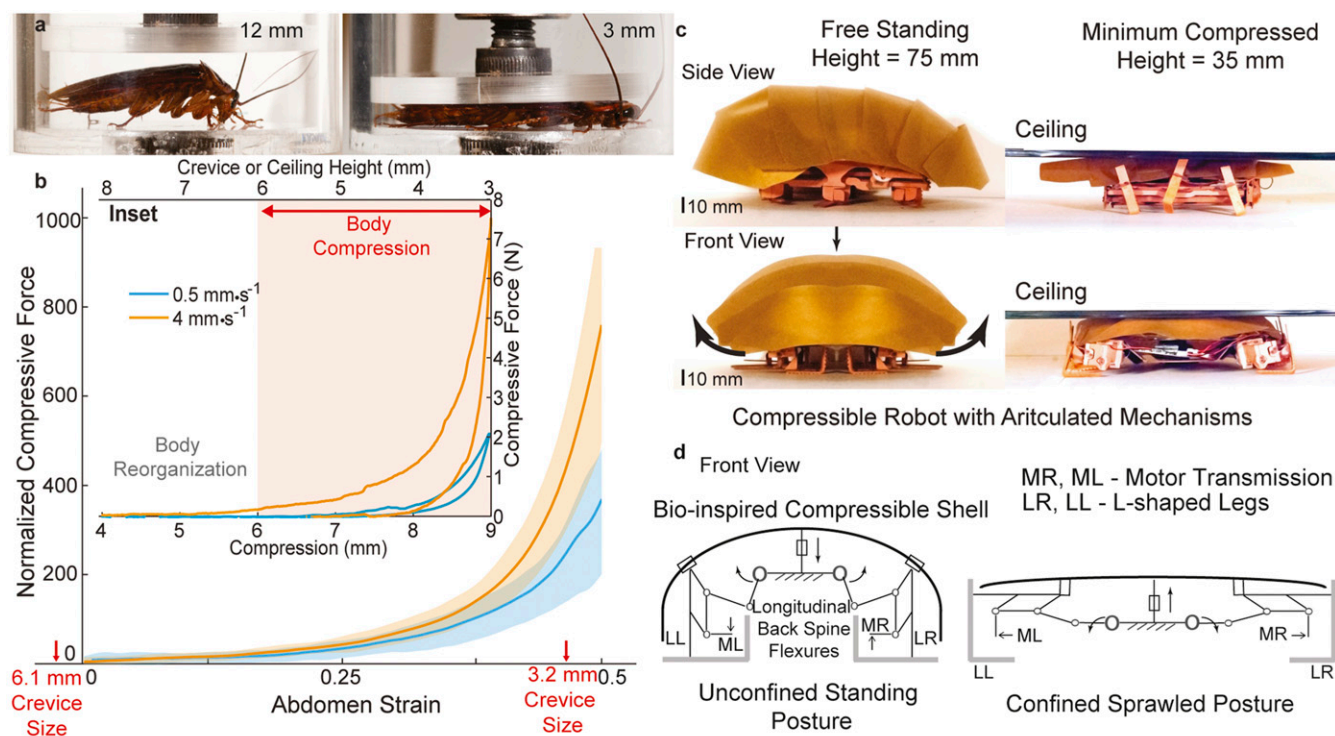

Fig. 5. Material properties of cockroaches during compression and bioinspired robot. (*A*) Materials testing apparatus with custom-built chamber positioned atop load cell to measure force during cyclic compression (Movie S3). (*B*) Normalized body compressive force (measured force/body weight) as a function of crevice size (red) and abdomen strain (change in abdomen compression/maximum abdomen thickness). Abdominal strain increases from left to right corresponding to a decrease in crevice size. Blue lines show a compression rate of 0.5 mm·s⁻¹. Tan lines show rate of 4 mm·s⁻¹. Shaded bands represent 95% confidence limits. (*Inset*) Compressive force cycles as a function of body compression distance for two rates of compression. The corresponding crevice or ceiling height is shown for comparison. Areas within the loop represent the energy lost per cycle. (*C*) Prototype robot with adjustable sprawl and abdominal compression-inspired exoskeletal plate-like shell (Movie S4) Top row photos, Side view of freestanding and confined-space posture for robot between two surfaces with ceiling labeled. Bottom row photos, Front view of freestanding and confined-space posture for robot between two surfaces. Top black small arrow shows direction of compression, and bottom black arrows show leg sprawl direction when compressed. (*D*) Schematic of the robot with a bioinspired compressible shell to visualize the degrees of freedom in unconfined standing (*Left*) and confined sprawled (*Right*) postures. The robot uses inspiration from the cockroach, not only with respect to body compression but also by changes in leg posture, allowing effective contact by the foot (tarsus) when standing and the leg (tibia) when running in a confined space.

Dynamic Compressive Forces. As a first step toward quantifying the body's exoskeletal material properties that enable cockroaches to traverse crevices and crawl in confined spaces, we performed a series of dynamic compressive cycle tests on living animals (Fig. 5A and *SI Methods*). We hypothesized that compression of the body and legs would demonstrate nonlinear, viscoelastic behavior, suggesting that crevice crossing might be affected by rate and that the magnitude of peak compression forces would reveal the extent of exoskeletal robustness. Compressive force showed a nonlinear increase as compression increased (Fig. 5B and Movie S3). Maximum average stresses ranged from 3.74 ± 0.56 kPa (at 0.5 mm·s^{-1}) to 16.21 ± 3.20 kPa (at 4 mm·s^{-1}) and were associated with very large strains (up to 0.50). Tangent modulus in the linear strain region (0.475–0.50) ranged from 0.11 ± 0.02 MPa (at 0.5 mm·s^{-1}) to 0.50 ± 0.10 MPa (at 4 mm·s^{-1}). The cockroach body behaved like a viscoelastic material with a resilience (percentage of energy return) of 60 ± 12% (at 0.5 mm·s^{-1}) and 44 ± 10% (at 4 mm·s^{-1}). At the smallest crevice or ceiling height of 3.2 mm, the net normal force (2.25 ± 1.17 N) on cockroaches averaged ~300 times body weight (Fig. 5B). This is significantly higher than forces recorded in soft-bodied annelids that experience about 10 times body weight when compressed to 0.6 body diameter (60), indicating the exceptional capability of the exoskeleton. At the faster rate of compression, net forces (6.08 ± 1.61 N) attained values of 700 times body weight with a maximum of ~900 times. We observed no damage to any body part. After the tests, cockroaches were able to fly normally and showed no significant changes in unconstrained running velocity (76.67 ± 7.34 cm·s^{-1}) compared with controls [$P = 0.49$, $F_{(1,35)} = 6.21$]. The relatively lower strain and higher buckling stiffness (3.36 GPa) measured in fresh sclerotized locust tibia (61) suggest the cockroach's compressibility derives from their soft arthrodial membranes rather than compression or bending of stiff exoskeletal plates (41) or tubes (36).

Soft Robot with Legs. Our discoveries from cockroaches inspired the design of a soft, legged hexapod robot named "compressible robot with articulated mechanisms" (CRAM) that we built using the SCM manufacturing approach (44–46) involving laser-cutting, laminating, and the folding of exoskeletal-like plates (Fig. 5 C and D, and *SI Methods*). Like the animal, the robot successfully locomotes in vertically confined spaces by compressing its body in half (54%; 75–35 mm) and benefits from possessing a low friction shell (Movie S4). Although the fluid-filled hemocoel in the animal imposes constraints on how the body deforms (i.e., compression along one axis forces expansion along the remaining axis by fixed proportions governed by the bulk modulus), the robot is free of such restrictions allowing it to expand, for example, along the horizontal plane when confined vertically. The robot shell can withstand compressive forces (1-kg weight) 20 times body mass by benefitting from overlapping abdominal plates and dissipate impacts and collisions demonstrating capabilities of robots constructed using soft materials (62–64). This prototype can increase sprawl angle (50° to 81°) by using compliant exoskeletal flexures to conform to the confined environment. Inspired by the cockroach, the terminal foot or tarsal-like segment is used for unconstrained running, whereas sprawling positions the leg or tibial-like segment for effective contact during compressed crawling (Movie S4). The advantages of dedicated propulsive appendages in compliant robots are clearly demonstrated by nearly an order of magnitude faster forward sustained speeds (both absolute, 14 cm·s^{-1}, and relative to body length, 0.75 bl·s^{-1}) compared with current state-of-the-art robotic crawlers (28, 63, 65, 66) despite large body compression. Future directions include addition of feet-like attachment mechanisms onto an upgraded leg design to improve peak forward velocity, control of leg actuation to improve energy efficiency (67), and the demonstration of new capabilities like turning (66), climbing (68), and jumping (64).

As Rus and Tolley (69) pointed out, "many of the exciting applications for soft robotics (such as search-and-rescue operations or environmental monitoring) require an autonomous, mobile system." A major limitation for current soft robots is that they rely on power and/or control signals delivered through pneumatic (28) and/or electric tethers (65, 66), making them very heavy [for example, 1.2 kg (63)]. By relying on SCM manufacturing techniques that have proved highly successful in the design of a fast running hexapedal family of robots (70, 71), we have been able to make our palm-sized, confined-space crawling robot completely autonomous in power and control, while weighing just 46 g including onboard electronics and battery. A promising future direction for soft-arthropod–inspired legged robots is to combine the advantages of soft-bodied robots (26, 69) with appendages shown to be effective in tubular environments such as gastrointestinal tracts (68). Our bioinspired soft-robot prototype presented here is a first step toward a search-and-rescue robot that can perform crevice traversal and confined-space body-friction legged crawling in an effort to rapidly locate survivors.

Methods

Crevice Traversal. We designed a custom apparatus to quantify the traversal behavior and time. The chamber consisted of clear acrylic plates with a vertically adjustable gate at one end (Fig. S1A). The inside of the entrance chamber was lined with 40-grit sandpaper to ensure effective footholds. Based on exoskeletal body compression measurements, we set the gate height at 3.2, 4.4, and 6.1 mm. We collected 315 trials from four individuals, classified them as (i) success, (ii) failure–turn back, or (iii) failure–stuck, and analyzed the 100 successful traversals (Fig. 1).

Confined-Space Crawling. We built a second custom apparatus for confined-space crawling that consisted of a closed, horizontal clear acrylic track with a vertically adjustable ceiling height (4–12 mm; Fig. S1B). For the first set of kinematic experiments consisting of 104 trials of five individuals each tested at 4, 6, 9, and 12 mm, we lined the inside bottom surface of the track with 40-grit sandpaper, whereas the inside top surface was acrylic. In a second set of experiments consisting of 638 trials on 10 individuals, we varied ceiling and ground friction based on our direct measurements for four ceiling heights. We present the 4-mm ceiling height data for 155 trials on 10 individuals (Fig. 3). In one condition, we varied ceiling kinetic friction from 0.09 to 0.46, while the ground kinetic friction was kept constant at 1.73. In the other condition, we varied ground kinetic friction on the body from 0.37 to 0.76 and from 0.84 to 2.04 on the legs (tibial spines), while the ceiling kinetic friction was kept constant at 0.16. We measured velocity, stride length and period, and stride success ratio. Based on our results, we developed a model of body-friction legged crawling (Fig. 4 and *Supporting Information*).

Dynamic Compressive Forces. We constructed a clear acrylic cylindrical chamber with the top attached to a freely sliding ceiling and the bottom mounted directly onto a universal materials testing machine load cell (Fig. 5A). We tested five live animals 10 times at two compression speeds, 0.5 and 4 mm·s^{-1}, over a range of compression values matching those experienced by animals in crevice traversal and confined-space crawling. We constructed force–compression curves, noted maximum net force, determined stiffness, and calculated resilience.

Soft Robot with Legs. We built a robot that uses a combination of postural adjustment from leg reorientation and body compression to locomote in vertically confined spaces, based on the cockroach data. The key design innovation making this possible is a flexible back spine coupled with a deformable shell made of overlapping plates similar to the exoskeletal plates of a cockroach abdomen (Fig. 5 C and D, Movie S4, and *Supporting Information*). The design of the robot is realized using the SCM manufacturing technique (44–46).

1. Li C, Zhang T, Goldman DI (2013) A terradynamics of legged locomotion on granular media. *Science* 339(6126):1408–1412.
2. Dickinson MH, et al. (2000) How animals move: An integrative view. *Science* 288(5463):100–106.
3. Sponberg S, Full RJ (2008) Neuromechanical response of musculo-skeletal structures in cockroaches during rapid running on rough terrain. *J Exp Biol* 211(Pt 3):433–446.
4. Spence AJ, Revzen S, Seipel J, Mullens C, Full RJ (2010) Insects running on elastic surfaces. *J Exp Biol* 213(11):1907–1920.
5. Spagna JC, Goldman DI, Lin P-C, Koditschek DE, Full RJ (2007) Distributed mechanical feedback in arthropods and robots simplifies control of rapid running on challenging terrain. *Bioinspir Biomim* 2(1):9–18.
6. Marvi H, et al. (2014) Sidewinding with minimal slip: Snake and robot ascent of sandy slopes. *Science* 346(6206):224–229.
7. Li C, Hsieh ST, Goldman DI (2012) Multi-functional foot use during running in the zebra-tailed lizard (*Callisaurus draconoides*). *J Exp Biol* 215(Pt 18):3293–3308.
8. Mazouchova N, Umbanhowar PB, Goldman DI (2013) Flipper-driven terrestrial locomotion of a sea turtle-inspired robot. *Bioinspir Biomim* 8(2):026007.
9. Li C, et al. (2015) Terradynamically streamlined shapes in animals and robots enhance traversability through densely cluttered terrain. *Bioinspir Biomim* 10(4):046003.
10. Hosoi AE, Goldman DI (2015) Beneath our feet: Strategies for locomotion in granular media. *Annu Rev Fluid Mech* 47:431–453.
11. Goldman DI, Chen TS, Dudek DM, Full RJ (2006) Dynamics of rapid vertical climbing in cockroaches reveals a template. *J Exp Biol* 209(Pt 15):2990–3000.
12. Autumn K, et al. (2002) Evidence for van der Waals adhesion in gecko setae. *Proc Natl Acad Sci USA* 99(19):12252–12256.
13. Autumn K, Dittmore A, Santos D, Spenko M, Cutkosky M (2006) Frictional adhesion: A new angle on gecko attachment. *J Exp Biol* 209(Pt 18):3569–3579.
14. Dai Z, Gorb SN, Schwarz U (2002) Roughness-dependent friction force of the tarsal claw system in the beetle *Pachnoda marginata* (Coleoptera, Scarabaeidae). *J Exp Biol* 205(Pt 16):2479–2488.
15. Dorgan KM (2015) The biomechanics of burrowing and boring. *J Exp Biol* 218(Pt 2):176–183.
16. Dorgan KM, Jumars PA, Johnson B, Boudreau BP, Landis E (2005) Burrowing mechanics: Burrow extension by crack propagation. *Nature* 433(7025):475.
17. Maladen RD, Ding Y, Li C, Goldman DI (2009) Undulatory swimming in sand: Subsurface locomotion of the sandfish lizard. *Science* 325(5938):314–318.
18. Gravish N, Monaenkova D, Goodisman MA, Goldman DI (2013) Climbing, falling, and jamming during ant locomotion in confined environments. *Proc Natl Acad Sci USA* 110(24):9746–9751.
19. Evans MEG (1977) Locomotion in Coleoptera Adephaga, especially Carabidae. *J Zool Lond* 181:189–226.
20. Calisti M, et al. (2011) An octopus-bioinspired solution to movement and manipulation for soft robots. *Bioinspir Biomim* 6(3):036002.
21. Reichman O, Smith SC (1990) Burrows and burrowing behavior by mammals. *Curr Mammal* 2:197–244.
22. Maladen RD, Ding Y, Umbanhowar PB, Goldman DI (2011) Undulatory swimming in sand: Experimental and simulation studies of a robotic sandfish. *Int J Robot Res* 30:793–805.
23. Trueman ER (1975) *The Locomotion of Soft-Bodied Animals* (American Elsevier Publishing, New York).
24. Trimmer BA, Lin HT (2014) Bone-free: Soft mechanics for adaptive locomotion. *Integr Comp Biol* 54(6):1122–1135.
25. Winter AG, et al. (2014) Razor clam to RoboClam: Burrowing drag reduction mechanisms and their robotic adaptation. *Bioinspir Biomim* 9(3):036009.
26. Kim S, Laschi C, Trimmer B (2013) Soft robotics: A bioinspired evolution in robotics. *Trends Biotechnol* 31(5):287–294.
27. Trivedi D, et al. (2008) Soft robotics: Biological inspiration, state of the art, and future research. *Appl Bionics Biomech* 5:99–117.
28. Shepherd RF, et al. (2011) Multigait soft robot. *Proc Natl Acad Sci USA* 108(51):20400–20403.
29. Laschi C, Cianchetti M (2014) Soft robotics: New perspectives for robot bodyware and control. *Front Bioeng Biotechnol* 2:3.
30. Lipson H (2014) Challenges and opportunities for design, simulation, and fabrication of soft robots. *Soft Robot* 1(1):21–27.
31. Full RJ, Tu MS (1991) Mechanics of a rapid running insect: Two-, four- and six-legged locomotion. *J Exp Biol* 156:215–231.
32. Full RJ, Tullis A (1990) Energetics of ascent: Insects on inclines. *J Exp Biol* 149:307–317.
33. Larsen GS, Frazier SF, Fish SE, Zill SN (1995) Effects of load inversion in cockroach walking. *J Comp Physiol A Neuroethol Sens Neural Behav Physiol* 176(2):229–238.
34. Mongeau J-M, et al. (2012) Rapid inversion: Running animals and robots swing like a pendulum under ledges. *PLoS One* 7(6):e38003.
35. Vincent JF, Wegst UG (2004) Design and mechanical properties of insect cuticle. *Arthropod Struct Dev* 33(3):187–199.
36. Vincent JF (2002) Arthropod cuticle: A natural composite shell system. *Compos A Appl Sci* 33(10):1311–1315.
37. Fabritius H, et al. (2011) Chitin in the exoskeletons of arthropoda: From ancient design to novel materials science. *Chitin* 34:35–60.
38. Lin H-T, Dorfmann AL, Trimmer BA (2009) Soft-cuticle biomechanics: A constitutive model of anisotropy for caterpillar integument. *J Theor Biol* 256(3):447–457.
39. Wootton RJ (1999) Invertebrate paraxial locomotory appendages: Design, deformation and control. *J Exp Biol* 202(Pt 23):3333–3345.
40. Mongeau J-M, Demir A, Lee J, Cowan NJ, Full RJ (2013) Locomotion- and mechanics-mediated tactile sensing: Antenna reconfiguration simplifies control during high-speed navigation in cockroaches. *J Exp Biol* 216(Pt 24):4530–4541.
41. Clark AJ, Triblehorn JD (2014) Mechanical properties of the cuticles of three cockroach species that differ in their wind-evoked escape behavior. *PeerJ* 2:e501.
42. Delcomyn F (1971) The locomotion of the cockroach *Periplaneta americana*. *J Exp Biol* 54:443–452.
43. Ding Y, Sharpe SS, Masse A, Goldman DI (2012) Mechanics of undulatory swimming in a frictional fluid. *PLoS Comput Biol* 8(12):e1002810.
44. Hoover AM, Fearing RS (2008) A fast scale prototyping process for folded millirobots. *Proceedings of the IEEE/RSJ International Conference on Robotics and Automation, 2008* (IEEE, Piscataway, NJ), pp 1777–1778.
45. Hoover AM, et al. (2010) Bio-inspired design and dynamic maneuverability of a minimally actuated six-legged robot. *Proceedings of the Third IEEE RAS and EMBS International Conference on Biomedical Robotics and Biomechatronics (BioRob), 2010* (IEEE, Piscataway, NJ), pp 869–876.
46. Wood RJ, Avadhanula S, Sahai R, Steltz E, Fearing RS (2008) Microrobot design using fiber reinforced composites. *J Mech Des* 130(5):052304.
47. Balasubramanian R, Rizzi AA, Mason MT (2003) Legless locomotion for legged robots. *Proceedings of the IEEE/RSJ International Conference on Intelligent Robots and Systems, 2003* (IEEE, Piscataway, NJ), Vol 1, pp 880–885.
48. Harley CM, English BA, Ritzmann RE (2009) Characterization of obstacle negotiation behaviors in the cockroach, *Blaberus discoidalis*. *J Exp Biol* 212(Pt 10):1463–1476.
49. Full R, Ahn A (1995) Static forces and moments generated in the insect leg: Comparison of a three-dimensional musculo-skeletal computer model with experimental measurements. *J Exp Biol* 198(Pt 6):1285–1298.
50. Horner AM, Biknevicius AR (2010) A comparison of epigean and subterranean locomotion in the domestic ferret (*Mustela putorius furo*: Mustelidae: Carnivora). *Zoology (Jena)* 113(3):189–197.
51. Nichols EL, Franklin W (1898) *The Elements of Physics* (Macmillan, London), Vol 1, p 101.
52. Bobbert MF (2012) Why is the force-velocity relationship in leg press tasks quasi-linear rather than hyperbolic? *J Appl Physiol (1985)* 112(12):1975–1983.
53. Full R, Yamauchi A, Jindrich D (1995) Maximum single leg force production: Cockroaches righting on photoelastic gelatin. *J Exp Biol* 198(Pt 12):2441–2452.
54. Gorb SN, et al. (2002) Structural design and biomechanics of friction-based releasable attachment devices in insects. *Integr Comp Biol* 42(6):1127–1139.
55. Clemente CJ, Dirks JH, Barbero DR, Steiner U, Federle W (2009) Friction ridges in cockroach climbing pads: Anisotropy of shear stress measured on transparent, microstructured substrates. *J Comp Physiol A Neuroethol Sens Neural Behav Physiol* 195(9):805–814.
56. Arzt E, Gorb S, Spolenak R (2003) From micro to nano contacts in biological attachment devices. *Proc Natl Acad Sci USA* 100(19):10603–10606.
57. Federle W, Brainerd EL, McMahon TA, Holldobler B (2001) Biomechanics of the movable pretarsal adhesive organ in ants and bees. *Proc Natl Acad Sci USA* 98(11):6215–6220.
58. Federle W, Riehle M, Curtis AS, Full RJ (2002) An integrative study of insect adhesion: Mechanics and wet adhesion of pretarsal pads in ants. *Integr Comp Biol* 42(6):1100–1106.
59. Qian F, et al. (2015) Principles of appendage design in robots and animals determining terradynamic performance on flowable ground. *Bioinspir Biomim* 10(5):056014.
60. Quillin KJ (2000) Ontogenetic scaling of burrowing forces in the earthworm *Lumbricus terrestris*. *J Exp Biol* 203(Pt 18):2757–2770.
61. Dirks J-H, Taylor D (2012) Fracture toughness of locust cuticle. *J Exp Biol* 215(Pt 9):1502–1508.
62. Seok S, Onal CD, Wood R, Rus D, Kim S (2010) Peristaltic locomotion with antagonistic actuators in soft robotics. *Proceedings of the IEEE/RSJ International Conference on Robotics and Automation, 2010* (IEEE, Piscataway, NJ), pp 1228–1233.
63. Tolley MT, et al. (2014) A resilient, untethered soft robot. *Soft Robot* 1(3):213–223.
64. Bartlett NW, et al. (2015) SOFT ROBOTICS. A 3D-printed, functionally graded soft robot powered by combustion. *Science* 349(6244):161–165.
65. Umedachi T, Vikas V, Trimmer B (2013) Highly deformable 3-d printed soft robot generating inching and crawling locomotions with variable friction legs. *IEEE/RSJ International Conference on Intelligent Robots and Systems, 2013* (IEEE, Piscataway, NJ), pp 4590–4595.
66. Umedachi T, Trimmer B (2014) Design of a 3D-printed soft robot with posture and steering control. *Proceedings of the IEEE/RSJ International Conference on Robotics and Automation, 2014* (IEEE, Piscataway, NJ), pp 2874–2879.
67. Zhou X, Majidi C, O'Reilly OM (2014) Energy efficiency in friction-based locomotion mechanisms for soft and hard robots: Slower can be faster. *Nonlinear Dyn* 78(4):2811–2821.
68. Valdastri P, et al. (2009) A new mechanism for mesoscale legged locomotion in compliant tubular environments. *IEEE Trans Robot* 25(5):1047–1057.
69. Rus D, Tolley MT (2015) Design, fabrication and control of soft robots. *Nature* 521(7553):467–475.
70. Birkmeyer P, Peterson K, Fearing RS (2009) DASH: A dynamic 16g hexapedal robot. *IEEE/RSJ International Conference on Intelligent Robots and Systems, 2009* (IEEE, Piscataway, NJ), pp 2683–2689.
71. Haldane DW, Fearing RS (2015) Running beyond the bio-inspired regime. *Proceedings of the IEEE/RSJ International Conference on Robotics and Automation, 2015* (IEEE, Piscataway, NJ), pp 4539–4546.
72. Sharpe SS, Kuckuk R, Goldman DI (2015) Controlled preparation of wet granular media reveals limits to lizard burial ability. *Phys Biol* 12(4):046009.